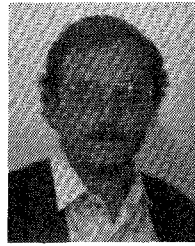




Luc Van den Bossche was born in Dendermonde, Belgium, on August 1, 1953. He received the degree of Technisch Ingenieur from the Technische Hogeschool SITO, Mechelen, Belgium.

In 1976 he joined Bell Telephone Manufacturing Company, Antwerp, Belgium, where he is working on linear and high-voltage integrated circuits.



Luc A. Bientman was born in Knokke, Belgium, on April 19, 1953. He received the degree of Technisch Ingenieur from the Technische Hogeschool HTISA, Gent, Belgium, and the E.E. degree from the Katholieke Universiteit Leuven, Belgium, in 1974 and 1977, respectively.

From 1977 to 1981 he was with the ESAT Laboratory, K.U. Leuven, Belgium, where he has been working towards the Ph.D. degree. Since 1981 he has been employed at Bell Telephone Manufacturing Company, Antwerp,

Belgium, and is presently working on BiMOS analog and digital design for telecom circuits.

Computer-Aided Distortion Analysis of Switched Capacitor Filters in the Frequency Domain

JOOS VANDEWALLE, SENIOR MEMBER, IEEE, JAN RABAAY, WARD VERCRUYSSSE,
AND HUGO J. DE MAN, SENIOR MEMBER, IEEE

Abstract—A Volterra series-based distortion analysis technique for switched capacitor circuits is presented. The algorithm has been implemented in the DIANA-SC program and is completely compatible with other DIANA simulation modes. The efficiency of the method is based on the use of direct z -domain and compaction methods, while only one extra circuit analysis is needed for each higher order distortion fraction of interest. Nonlinear operational amplifiers and capacitors can be handled using polynomial models. Both harmonic and intermodulation distortion analysis modes are available. The method is demonstrated using a practical design example.

I. INTRODUCTION

IN recent years, switched capacitor (SC) techniques have become very successful and have allowed the integration of a variety of signal processing circuits, such as speech synthesizers, audio, and PCM filters. The design of SC networks is, however, complicated by a large number of sampled data and parasitic effects, such as clock feedthrough, offset, stray capacitance and switch on-resistance, aliasing and sample-and-hold effects, band-limited operational amplifiers, and noise. All these effects cannot efficiently be analyzed using pen and paper methods. This motivates the intensive research spent during recent years to the development of efficient CAD tools for SC circuit design [1].

Manuscript received October 13, 1982; revised December 21, 1982.

J. Vandewalle and H. J. De Man are with ESAT Laboratory, Katholieke Universiteit Leuven, Heverlee, Belgium.

J. Rabaey is with the Belgian National Fund for Scientific Research, Heverlee, Belgium, and also with the Katholieke Universiteit Leuven, Heverlee, Belgium.

W. Verduyck is with the Katholieke Universiteit Leuven, Heverlee, Belgium. He is now with Silvar-Lisco, Heverlee, Belgium.

Most of these computer implementations, however, handle only ideal, linear, resistorless SC networks and do not deal with the effects of band-limited operational amplifiers on the frequency domain behavior or with noise and distortion analysis. However, the signal-to-noise (S/N) ratio is of extreme importance in the design of audio filters and is determined by the noise level on the one hand, and the distortion level on the other. A limited number of noise analysis techniques have been presented up to now [2], [3] and an efficient and general noise simulator has also been implemented in the DIANA-SC program [4], based on the resistive SC simulation level [5]. The domain of the frequency domain distortion, however, has hardly been explored until now, with the exception of a technique presented by Davis [6].

In this paper, a technique for the distortion analysis of weakly nonlinear switched capacitor circuits using the discrete Volterra series is presented using the same basic principles as those in [6]. Much efficiency is obtained by combining it with the fast frequency domain analysis of linear switched capacitor networks [7], [8] (extended modified nodal analysis (MNA) matrix, direct z -domain method, adjoint switched capacitor and compaction techniques, and sparse matrix methods). A restriction to the presented algorithm is that, for distortion analysis, only ideal SC networks are handled in the sense that the effects of parasitic resistances and continuous input-output (I/O) couplings are ignored.

After a short overview of the DIANA-SC strategy and basic principles, a brief description of the algorithm is given, followed by a detailed discussion of the nonlinear sources present in SC networks and their modeling. The paper concludes with

TABLE I
SIMULATION LEVELS AND MODES IN DIANA-SC

DIANA - SC		
LEVEL	TIME	FREQUENCY
TOP ideal sc circuits without resistors	impulse responses step & sinusoidal resp offset non-linear drift	frequency domain T F aliasing T F sensitivities group delay DISTORTION
INTERM. sc-circuits including resistive effects	clock-feedthrough bandlimited opamps transient effects sinusoidal response	frequency domain T F including effects of bandlimited opamps and switch resistances Noise
DOWN full mos mixed mode	opamp-design mixed mode analog filter + digital control	

an overview of distortion definitions (harmonic and intermodulation distortion), their relation with the DIANA outputs, and an illustration of a detailed simulation of a third-order elliptical low-pass filter.

II. THE DIANA-SC CONCEPT: AN OVERVIEW

Before we go on to a detailed description of the distortion analysis, an overview of the strategy and some basic concepts of DIANA are indispensable. Table I displays the different levels available and demonstrates the use of DIANA as a “top-down” design tool for SC circuits [9], [10]. This means that, in analogy with digital networks, the design of an SC circuit is started from idealized networks (linear, no parasitics, no resistors). After initial design checking, simulation continues on a more detailed level, including the effects of switch resistances and capacitors, band-limited operational amplifiers, stray capacitances, clock feedthrough, noise, and even full MOS transistor models and mixed mode simulation (only in the time domain). Obviously, one has to take into account the “decreasing abstraction level, increasing computer cost” principle. Most of these algorithms are already described in literature [4], [5], [7], [8].

Since the solution of nonlinear SC networks is, however, based on a repetitive solution of a number of linearized networks, a short description of the analysis techniques for linear, resistorless SC systems is needed. At this point, we consider only piece-wise constant inputs—the main reason is that the superposition principle used to handle the effects of the continuous couplings in linear networks is not valid in nonlinear networks.

Consider an n -phase T -periodic linear SC network N_s . For each clock phase k ($k = 1, \dots, N$), a set of difference equations using the MNA description can be set up:

$$\mathbf{M}_k \cdot \mathbf{x}_k(nT + t_k) = \mathbf{N}_k \cdot \mathbf{x}_{k-1}(nT + t_{k-1}) + \mathbf{e}_k(nT + t_k) \quad (1)$$

$$n = 1, 2, \dots, N$$

with \mathbf{M}_k the MNA matrix, \mathbf{N}_k the nodal capacitance matrix, \mathbf{x}_k the vector of nodal voltages and branch currents at the end of clock phase k (time point $t_k + nT$, with T the period) and \mathbf{e}_k the excitation vector.

Efficient frequency domain simulations are feasible, combining the time domain equations in (1) for all clock phases and transforming them to the z -domain. This results in an augmented set of z -domain equations in (2), describing an invariant network with an extended MNA matrix:

$$\begin{bmatrix} \mathbf{M}_1 & & & & -\mathbf{N}_1 z^{-1} \\ & \mathbf{M}_2 & & & \\ & & \ddots & & \\ & & & -\mathbf{N}_N & \mathbf{M}_N \end{bmatrix} \begin{bmatrix} \mathbf{X}_1(z) \\ \mathbf{X}_2(z) \\ \vdots \\ \mathbf{X}_N(z) \end{bmatrix} = \begin{bmatrix} \mathbf{E}_1(z) \\ \mathbf{E}_2(z) \\ \vdots \\ \mathbf{E}_N(z) \end{bmatrix} \quad (2)$$

or

$$\mathbf{M}(z) \cdot \mathbf{X}(z) = \mathbf{E}(z). \quad (3)$$

Solving (3) (inverting $\mathbf{M}(z)$ using classical sparse matrix methods and exploiting the special nature of the extended MNA matrix) results in a matrix of z -domain transfer functions, called the z -domain transfer matrix. The final frequency domain behavior (transfer functions and aliasing terms) are then easily obtained, by converting the results of (3) to the frequency domain ($z = \exp(j\omega t)$) and combining the different terms with the appropriate phase shifts and sample-and-hold effects ($\sin(x)/x$). For more mathematical details about the above method, the reader is referred to [7].

III. NONLINEAR DISTORTION ANALYSIS USING VOLTERRA SERIES

When browsing through the literature, it becomes clear that different distortion analysis methods developed for analog networks can be adapted for the analysis of discrete time networks:

1) A first method consists of a calculation in the time domain of the steady-state response to a sinusoidal excitation, using a Newton-Raphson iteration in each clock interval [10], followed by a transformation into the frequency domain using a DFT algorithm. This technique is used in a number of classical simulators (e.g., SPICE [11] using the Fourier mode), but tends to be CPU time consuming in filter analysis, especially for filters with a high Q .

2) Direct frequency methods as the perturbation method [12] and the Volterra series method [13], [14] are much more efficient. The Volterra series method is favorable due to the close relations between the higher order Volterra terms and the harmonic distortion products and also due to the simple computation of the harmonics when changing the input excitation magnitude. The method proved to be successful for the analysis of bipolar networks [15] and is also implemented in SPICE for analog networks (use of the DISTO mode) [19].

The basic principles of the algorithm will be made clear using the example of the two phase RC low-pass SC filter of Fig. 1(a). The nonlinear capacitor C_3 has a charge-voltage relation $q_3 = f(v_3)$.

The Volterra series method can now easily be adapted to handle time-discrete systems (as shown also in [6]) and fits perfectly into the DIANA framework as presented in Section II. The method is based on two assumptions.

1) The nonlinear elements relations can be approximated us-

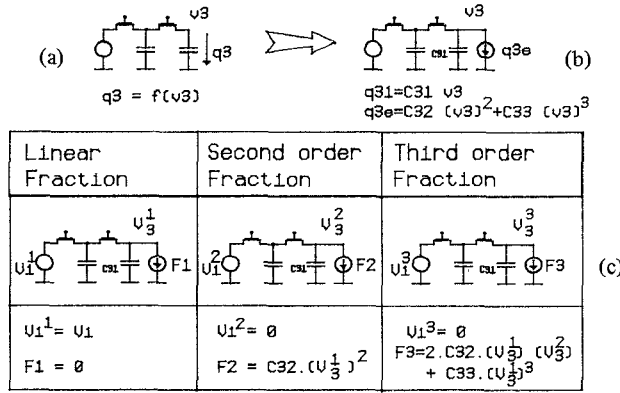


Fig. 1. The Volterra approach applied on passive SC network. (a) Polynomial expansion. (b) Subsequent analysis of linearized networks with (c) appropriate error sources.

ing polynomial expressions, e.g., the charge-voltage relation of the nonlinear capacitor in Fig. 1(a): $q_3 = C31 \cdot v + C32 \cdot v^2 + C33 \cdot v^3 + \dots$

This immediately imposes a restriction—the method is only valid for weakly nonlinear circuits with limited signal magnitudes, as the nonlinearities have to be approximated by a polynomial expression around the dc operation points. The statement shows that the presented analysis technique will rather lead to *educated approximations* of the nonlinear network behavior than to extreme accuracy. These restrictions are identical to the limitations of the SPICE distortion analysis mode (for purely analog networks).

2) All network signals can be written as Volterra series with respect to the input signals

$$\mathbf{x}_k(nT + t_k) = \sum_{m=1}^{\infty} \mathbf{x}_{k,m}(nT + t_k) \quad (4)$$

where $\mathbf{x}_{k,m}$, called the m th-order term, is determined by a m -dimensional discrete convolution of m copies of the input signal with a so-called Volterra kernel (or m -dimensional impulse response). A direct consequence from this is that multiplication of the input signal with a scaling factor results in

$$\mathbf{x}_k(nT + t_k) = \sum_{m=1}^{\infty} \epsilon^m \mathbf{x}_{k,m}(nT + t_k). \quad (5)$$

Adapting the strategy for analog networks [14] to n -phase T -periodic networks, we obtain the following analysis procedure.

1) Set up the MNA equations for all clock phases and express all nonlinear elements as functions of their polynomial expressions. Transfer all higher order terms to the right-hand side (function f), keeping only the linear terms at the left-hand side. For clock phase k ,

$$\mathbf{M}_k \cdot \mathbf{x}_k - \mathbf{N}_k \cdot \mathbf{x}_{k-1} = \mathbf{e}_k + f(\mathbf{x}_k, \mathbf{x}_{k-1}). \quad (6)$$

Note that \mathbf{M}_k is the MNA matrix of the linearized network. The above procedure is demonstrated in Fig. 1(b) for the example.

2) Express all variables as functions of their Volterra expansion

sions [using (4)]

$$\begin{aligned} \mathbf{M}_k \sum_{m=1}^{\infty} \epsilon^m \mathbf{x}_{k,m} - \mathbf{N}_k \sum_{m=1}^{\infty} \epsilon^m \mathbf{x}_{k-1,m} \\ = \epsilon \mathbf{e}_k + \sum_{m=2}^{\infty} \epsilon^m \cdot f_{k,m}. \end{aligned} \quad (7)$$

The following important features can be noticed.

The last summation of (7) is called a nonlinear source or “error term” and concentrates the nonlinear effects. Note that no linear term is present in this error term.

The m th order error term F_m is only a function of the $\mathbf{x}_{i,m-1}, \dots, \mathbf{x}_{i,1}$ ($i = k, k-1$) or is only determined by lower order Volterra fractions.

3) Transform (7) to the z -domain [identical to (2)], obtaining one single z -domain equation:

$$\mathbf{M} \cdot \sum_{m=1}^{\infty} \epsilon^m \mathbf{X}_m(z) = \epsilon \mathbf{E}(z) + \sum_{m=2}^{\infty} \epsilon^m \mathbf{F}_m(z). \quad (8)$$

Solve (8) subsequently for $m = 1, 2, \dots$ (dependent upon the number of higher order terms of interest) as shown in (9) and in Fig. 1(c) for the example of Fig. 1(a). After each analysis, calculate the error source $\mathbf{F}_{m+1} = g(\mathbf{X}_m, \mathbf{X}_{m-1}, \dots, \mathbf{X}_1)$ for the next higher order analysis

$$\begin{aligned} \mathbf{M}(z) \cdot \mathbf{X}_1(z) &= \mathbf{E}(z) && \text{linear} \\ \mathbf{M}(z) \cdot \mathbf{X}_2(z) &= \mathbf{F}_2(\mathbf{X}_1) && \text{second-order} \\ \mathbf{M}(z) \cdot \mathbf{X}_3(z) &= \mathbf{F}_3(\mathbf{X}_2, \mathbf{X}_1) && \text{third-order.} \\ &\vdots && \end{aligned} \quad (9)$$

The algorithm, set up in this way, is very efficient since all analyses are based on the inversion of the same, linearized extended, MNA matrix \mathbf{M} , changing only the excitation vector. Storage, ordering, and partial LU decomposition of \mathbf{M} need only to be performed once. It is clear that the algorithm is perfectly compatible with the frequency domain analysis mode of ideal, linear SC networks.

Also important is that all higher order terms \mathbf{X}_m are directly proportional to the m th power of the fundamental (or linear) signals and that all harmonic and intermodulation products can be computed in function of the \mathbf{X}_m .

The remaining task is to derive the expressions for the error sources $\mathbf{F}_2, \mathbf{F}_3, \dots$ in explicit form. These expressions are, however, dependent upon the type of the input waveform and are different for exponential, cosinusoidal, or mixed inputs. As a full derivation of these cases would lead us too far, we limit ourselves to the case of an exponential input and a nonlinear voltage controlled voltage source (VCVS). For a more detailed description of the derivations for other input waveforms and other elements, we refer to [16].

Consider a nonlinear VCVS between node m and ground, which is controlled by the voltage between node i and ground. This causes the following branch relation in the MNA description (for clock phase k):

$$[v^{(m)}(nT + t_k)] - A1 \cdot [v^{(i)}(nT + t_k)] = \hat{f}(nT + t_k)$$

with

$$\hat{f}(nT + t_k) = A2 \cdot [v^{(i)}(nT + t_k)]^2 + A3 \cdot [v^{(i)}(nT + t_k)]^3 + \dots \quad (10)$$

Introduce the Volterra series expansions in the way described in (5):

$$v^{(p)}(nT + t_k) = v_k^{(p)}(n) = \sum_{r=1}^{\infty} v_{k,r}^{(p)}(n) \cdot \epsilon^r. \quad (11)$$

The fractions of the error functions can be found by equating identical powers of ϵ

$$\hat{f}_{k,1}(n) = 0 \quad (12a)$$

$$\hat{f}_{k,2}(n) = A2 \cdot (v_{k,1}^{(i)})^2 \quad (12b)$$

$$\hat{f}_{k,3}(n) = 2 \cdot A2 \cdot (v_{k,2}^{(i)})(v_{k,1}^{(i)}) + A3 \cdot (v_{k,1}^{(i)})^3. \quad (12c)$$

⋮

Suppose that the network is excited with an exponential input

$$e_k(t) = \hat{E} \cdot \sum_{n=-\infty}^{\infty} e^{j\omega_0(nT + t_k)} \cdot \delta(t - nT - t_k) \quad (13)$$

or in the frequency domain

$$E_k(\omega) = \hat{E} \sum_{n=-\infty}^{\infty} e^{j\omega t_k} \cdot \delta(\omega - \omega_0 - n\omega_s). \quad (14)$$

Exciting the linearized network with (14) results in following general form solution [from (9)]

$$X_{k,1} = \hat{X}_{k,1} \sum_{n=-\infty}^{\infty} \delta(\omega - \omega_0 - n\omega_s). \quad (15)$$

The second-order error function can now be computed by applying the following strategy: transform (15) to the time domain, insert the result in (12b) and transform back to the frequency domain. This yields the second-order error source

$$F_2(\omega) = \frac{2\pi}{T} \cdot A2 \cdot (\hat{v}_{k,i}^{(i)}) \cdot \sum_{n=-\infty}^{\infty} \delta(\omega - 2\omega_0 - n\omega_s). \quad (16)$$

The same procedure can be applied for the derivation of the higher order error sources or for other input waveforms and nonlinear elements.

IV. MODELING OF NONLINEAR SOURCES

Nonlinear distortion is introduced in SC circuits through several sources. The most important distortion sources are discussed here and polynomial models are set up.

Nonlinear Junction Capacitances of MOS Switches [Fig. 2(a)]: These diode capacitances become especially important in nonparasitic free SC networks, where they are placed in parallel with the filter capacitances and enter directly into the frequency domain transfer functions. The use of parasitic-free SC networks diminishes the effects of the junction capacitances on the frequency domain behavior and suppresses the nonlinear distortion, introduced by the elements.

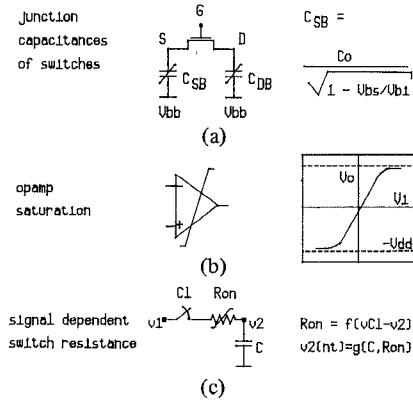


Fig. 2. Distortion sources in SC networks. (a) Junction capacitors. (b) Op amp saturation. (c) Switch resistors.

A possible nonlinear model for the junction capacitances can be found using a Taylor series expansion of the $q(V)$ characteristic (17) around the dc operation point

$$q(V) = K \cdot [\sqrt{1 - V/V_{bi}} - 1] \quad (17)$$

with V_{bi} the built-in diode voltage (0.6 V) resulting in the small signal polynomial expression (18)

$$q(V) = q(V_{dc}) + C1 \cdot (v + C2 \cdot v^2 + C3 \cdot v^3 + \dots) \quad (18)$$

with

$$v = V - V_{dc}$$

and

$$C1 = C0 / \sqrt{1 + V_{dc}/V_{bi}}$$

$$C2 = (\frac{1}{4}) \cdot 1 / (V_{bi} - V_{dc})$$

$$C3 = (\frac{1}{8}) \cdot 1 / (V_{bi} - V_{dc})^2.$$

⋮

The higher order terms are only dependent upon the dc operation point, so that all capacitors with the same dc value can use the same nonlinear model. There is no need to evaluate the dc term $q(V_{dc})$ as only charge differences are of importance in the algorithm. In Fig. 3, a number of polynomial approximations for different dc values are plotted. Note also that this capacitor model can be replaced easily by a user defined model, which is more related to the applied IC technology.

Saturation Characteristic of Operational Amplifiers [Fig. 2(b)]: This distortion characteristic can be considered as the most important in practical SC networks, especially for higher signal values. As the saturation characteristic is normally symmetrical around the x-axis (especially in CMOS op amps), polynomial modeling contains only odd order terms (19)

$$V_o = A1 \cdot V_i \cdot (1 + A3 \cdot V_i^2 + A5 \cdot V_i^4 + \dots). \quad (19)$$

The coefficients can be found by polynomial regression on a measured saturation characteristic in the area of interest. Note, however, that in NMOS operational amplifiers, a non-symmetrical characteristic is possible, introducing even order harmonics. This is true for the operational amplifier described in [17] and used in the example in Section VI. The gain

Taylor series expansion around
operating point

$$Q(V) = C11 * (V + C12 * V * V + C13 * V * V * V)$$

with

$$C11 = Co / (1 - Udc/Ub1) * 0.5$$

$$C12 = 1 / 4 * (Ub1 - Udc)$$

$$C13 = 1 / 8 * (Ub1 - Udc) * 2$$

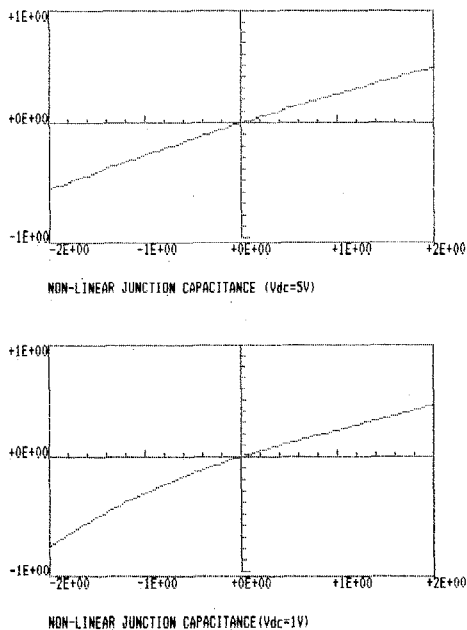


Fig. 3. Modeling of nonlinear junction capacitors.

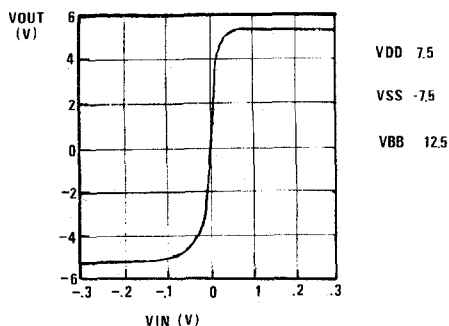


Fig. 4. Nonlinear op amp characteristic and polynomial modeling.

characteristic of this op amp and the coefficients of the polynomial approximation are given in Fig. 4.

A third form of distortion could occur when the on-resistance of the MOSFET switches R_{on} produces a time-constant τ in the charging of the switched capacitors, which is comparable

to the duration of the clock phase [Fig. 2(c)]. As R_{on} is highly dependent upon the gate to source voltage, τ and thus also the capacitor voltage, reached at the end of the time slot, is dependent upon the signal value in an exponential way. Since in most SC circuits the nodal voltages reach their equilibrium values, this distortion source can be ignored in almost all but very high frequency practical SC networks.

V. HARMONIC AND INTERMODULATION DISTORTION

Results of distortion measurements are always expressed in terms of the harmonic or the intermodulation distortion products. The relation between the higher order Volterra terms and the distortion products will be demonstrated here.

Harmonic Distortion: The n th-order harmonic distortion product is defined by exciting the network with a sinusoidal signal $V_i = V \cdot \cos(\omega t)$ and looking at the $n \cdot \omega$.

$$HDn = \frac{\text{amplitude of harmonic component at } n \cdot \omega}{\text{amplitude of fundamental at } \omega} \quad (20)$$

As a result of a Volterra series procedure with sinusoidal input, a number of higher order signal components are obtained as plotted in Fig. 5. Some of these contributions vary linearly in terms of the size of the input, others as a second order (quadratic), third order, and so on. The linear part contains contribution $A11$ (cosine amplitude) at the same frequency f as the input (fundamental) and at frequencies $f \pm k \cdot fs$ (aliasing terms) with $fs = 1/T$ the sampling frequency. These aliasing terms, which are normally negligible, are caused by the sampling nature of the SC network. The second-order part contains a contribution $A22$ (cosine amplitude) at $2 \cdot f$, a dc term $A20$ (drift) and aliasing terms, while the third-order term consists, besides the aliasing signals, of a contribution $A33$ at $3 \cdot f$ and $A31$ at the fundamental frequency f ($A31$ is normally smaller than $A11$). All these factors are obtained as output in the DIANA program.

The harmonic distortion products can now be calculated:

$$HD2 = \frac{|(A22 + A42 + \dots)|}{|(A11 + A31 + \dots)|} \approx |A22|/|A11|, \quad \text{for smaller input signals} \quad (21)$$

$$HD3 = \frac{|(A33 + A53 + \dots)|}{|(A11 + A31 + \dots)|} \approx |A33|/|A11|. \quad (22)$$

$A11$, $A22$, and $A33$ behave, respectively, as linear, quadratic, and cubic, with respect to the input, which means that $HD2$ and $HD3$, when plotted on a log-log scale in function of the input amplitude, have fixed slopes for small input signals. At a higher signal level, the curves bend up or downwards due to the influence of fourth- and fifth-order terms.

Intermodulation Distortion: Intermodulation distortion occurs when applying input signals of different frequencies to a nonlinear circuit. For an excitation $V_1 = V \cdot (\cos(\omega_1 t) + \cos(\omega_2 t))$, a number of beat frequencies are generated besides the harmonic terms, as plotted in Fig. 6 (aliasing frequencies are ignored). These intermodulation products are obtained directly from the Volterra series algorithm, exciting the network with the appropriate error terms.

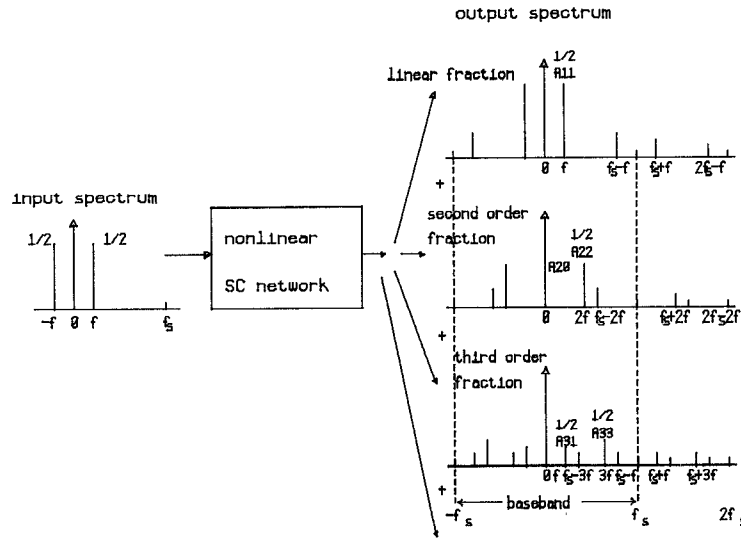


Fig. 5. Harmonic distortion factors in SC networks.

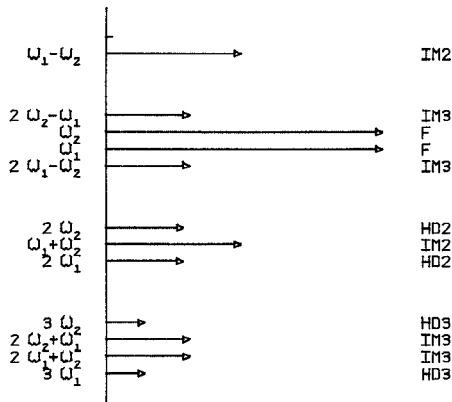


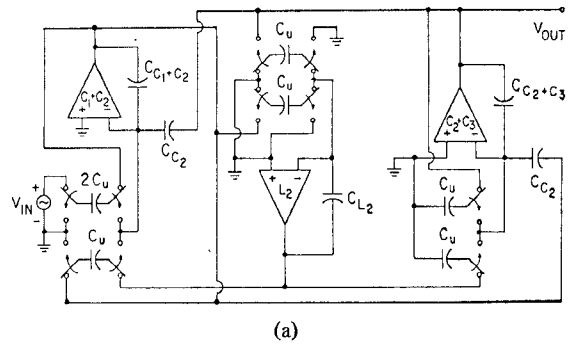
Fig. 6. Intermodulation distortion products.

VI. EXAMPLE

The efficiency and the accuracy of the method is demonstrated using the example of the third-order elliptical low-pass filter of Fig. 7 [17], [18] with the DIANA input description of Fig. 7(b). The simple introduction of the nonlinear elements in this description using the SCN model cards can be noted.

The DIANA-SC program is now used to compute the *S/N* ratio of the elliptical filter and to investigate the influence of the different nonlinear sources. At first, the noise behavior of the filter is simulated as shown in Fig. 8, where the frequency domain transfer function and the noise spectral density at the output (in dB/√Hz) are plotted. The close agreement with the measured response (from [17]) can be noted. The integrated noise in the interval 300 Hz–3 kHz equals 80 μV · rms.

The results of a distortion analysis of the filter are given in Fig. 9(a), where the different higher order terms (*A22*, *A33*, *A31*, *A20*, *A42*, *A53*) are plotted. These are combined into the second (*HD2*), third (*HD3*), and total (THD) harmonic terms, as shown in Fig. 9(b) for two different input frequencies. From this figure, it can be noted that the simulated THD



```

third order elliptical filter : nonlin analysis
.scfreq fstart=100 fstop=10K fsample=128k ndec=50 harm=5
print vo
input c1 clock=1 2 ic=1 cyc
input c2 clock=1 2 ic=0 cyc
|.scn amp 70.01 -12414.55 -1.6722meg, -47.995meg
|.scn junc 0.0191 -0.75r

$macro integr(#,ir,out,ag,cap)
xv# out 0 0 in ag amp
cint# out ir cap
cpi# ir 0 0.1p junc
cpi# out 0 0.1p junc
$end integr

$macro s4(#,n11,n12,n21,n22,cap)
s2#a n11 xa# c11 0 vt=1
s2#b n12 xa# c12 0 vt=1
s2#c n21 xb# c11 0 vt=1
s2#d n22 xb# c12 0 vt=1
cr#4 xa# xb# cap
cp4#1 xa# 0 0.1p junc
cp4#2 xb# 0 0.1p junc
$end s4

$macro s3(#,n11,n12,cap)
s2#e n11 xc# c11 0 vt=1
s2#f n12 xc# c12 0 vt=1
cr#3 xc# 0 cap
cp3# xc# 0 0.1p junc
$end s3

: circuit description
vin v1 0 1
call integr(1,2,3,923,18.90tp)
call integr(2,4,5,923,15.4838p)
call integr(3,6,vo,923,18.908tp)
call s4(1,v1,0,3,2,2.1223p)
call s4(2,4,0,0,vo,2.561p)
call s4(3,4,0,0,2,2.561p)
call s4(4,5,6,3,0,2.561p)
call s2(1,vo,6,2,561p)
call s2(2,vo,2,2,561p)
cnul1 2 vo 2 2.561p
cnul2 6 3 2.25p
.end
    
```

(b)

Fig. 7. (a) Third-order elliptical low-pass filter. (b) DIANA input.

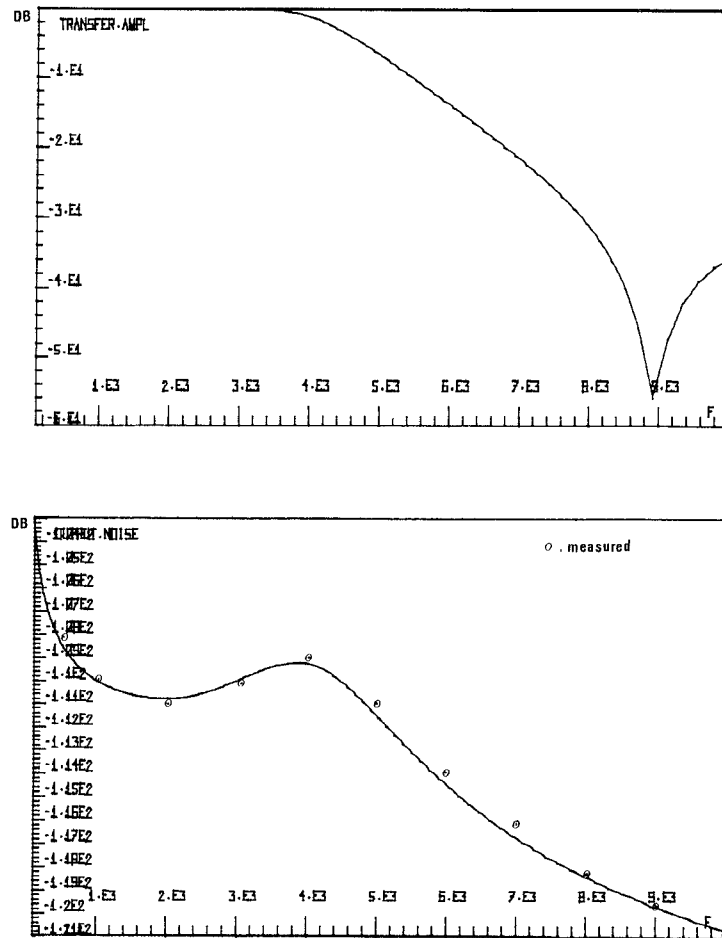


Fig. 8. Noise simulation on third-order elliptical low-pass filter of Fig. 7.

(total harmonic distortion) reaches the 0.1 percent value for an input signal of 1.15 V amplitude, while the 1 percent value is exceeded at 4.8 V · amp. Comparison with measurements shows that the simulation is rather accurate for smaller input signals (0.81 V · rms against ± 0.77 V · rms measured), but tends to deviate for higher input amplitudes: the measured 1 percent THD distortion value equals 2.6 V · rms or 3.677 V amplitude (compared to 4.8 V · amp). This is especially caused by the inaccuracy of the nonlinear op amp model near the saturation voltages, as this strong nonlinear (and also asymmetrical in this case) effect can only be partially modeled using polynomials. Note that the use of higher order polynomial series (>5) is not recommended due the oscillatory nature of these higher order regressions. The inaccuracy in question is inherent to the algorithm. The simulated S/N ratio equals 92.55 dB, compared to the measured 90 dB. The total simulation time for this network on VAX/VMS 11/780 was 26.5 s (100 frequency points).

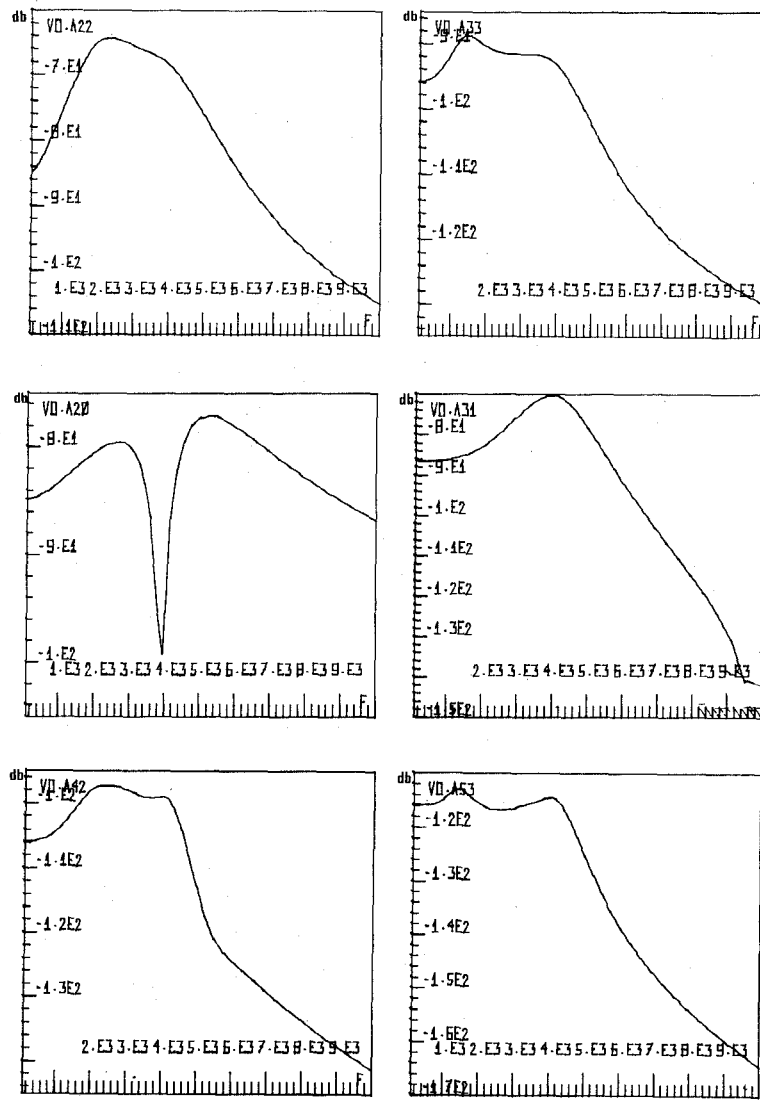
In Fig. 10, a comparison is made between the different nonlinear sources (input amplitude 1 V · amp). It can clearly be seen that the nonlinear junction capacitors are the most important distortion sources for this input signal. This is caused by the fact that this elliptical filter is sensitive to stray capacitances. The distortion behavior of the filter for lower input

signals could be improved quite a lot by using stray free SC equivalents. It can also be noted from Fig. 10 that the op amp distortion will become the most important distortion source at higher input amplitudes (through the third- and higher order fractions).

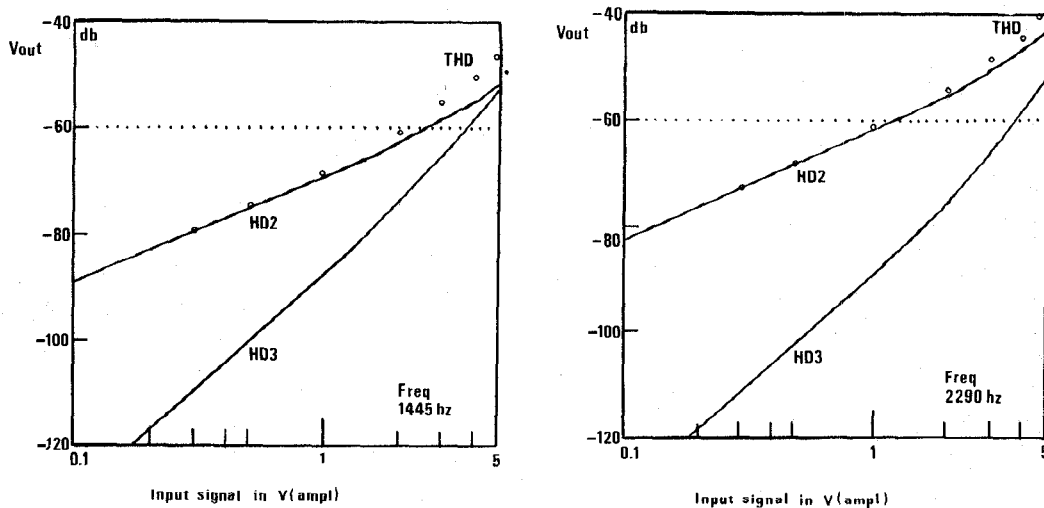
The above example demonstrates the capability of the presented simulator to give a reasonable prediction of the S/N ratio of an SC filter. It also allows for a clear insight in the influence and the importance of the different nonlinear sources.

VII. CONCLUSIONS

A method is presented to compute the distortion behavior of weakly nonlinear SC networks using Volterra series. The method handles N -phase resistorless SC networks with piecewise constant inputs, is directly compatible with other DIANA simulation modes, and is efficient since only one extra circuit analysis is needed per higher order term of interest. The applications of the simulation technique are restricted to the analysis of weakly nonlinear SC circuits with limited excitations due to the use of polynomial nonlinear models. Together with the noise analysis mode, implemented in DIANA, this distortion simulation mode allows for a reasonable prediction of the S/N ratio of a filter circuit.



(a)



(b)

Fig. 9. Distortion analysis of third-order elliptical low-pass filter. (a) Higher order fractions A22, A33, A20, A31, A42, A53. (b) Harmonic distortion terms at frequencies 1445 Hz and 2290 Hz ($\log V_{out} - \log V_{in}$).

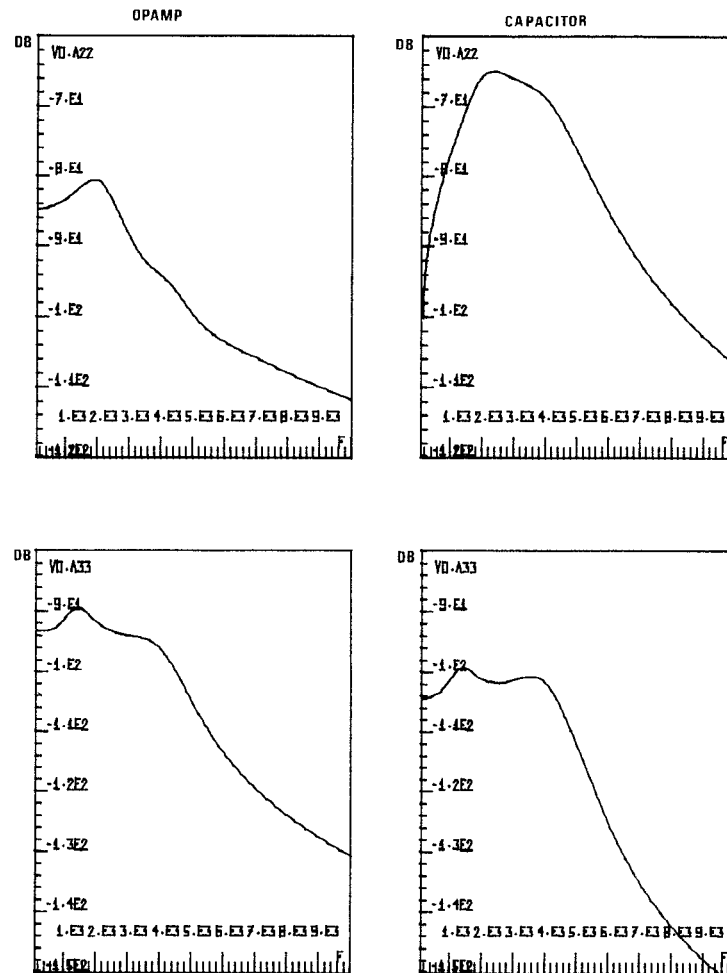


Fig. 10. Distortion sources in third-order elliptical filter: comparison (second- and third-order fractions).

REFERENCES

- [1] J. Rabaey, L. Claesen, H. De Man and J. Vandewalle, "An overview of CAD techniques for switched capacitor networks," in *Proc. ECCTD Conf.*, The Hague, The Netherlands, Aug. 1981, pp. 513-517.
- [2] B. Furrer and W. Guggenbuhl, "Noise analysis of sampled-data circuits," *AEU*, vol. 35, Ch. 11, pp. 426-430, 1981.
- [3] J. Fischer, "Noise sources and calculation techniques for switched capacitor filters," *IEEE J. Solid-State Circuits*, vol. SC-17, pp. 742-752, Aug. 1982.
- [4] J. Rabaey, J. Vandewalle, and H. De Man, "A general and efficient noise analysis technique for switched capacitor filters," in *Proc. IEEE ISCAS Conf.*, Newport Beach, RI, May 1983.
- [5] J. Rabaey, J. Vandewalle, and H. De Man, "On the frequency domain analysis of switched capacitor circuits including all parasitics," in *Proc. IEEE ISCAS Conf.*, Chicago, IL, Apr. 1981, pp. 868-871.
- [6] R. Davis, "Distortion analysis of switched capacitor filters," in *Proc. IEEE ISCAS Conf.*, Chicago, IL, 1981, pp. 876-879.
- [7] J. Vandewalle, H. De Man, and J. Rabaey, "Time, frequency, and z-domain modified nodal analysis of switched capacitor circuits," *IEEE Trans. Circuits Syst.*, vol. CAS-28, pp. 186-195, Mar. 1981.
- [8] J. Vandewalle, L. Claesen, and H. De Man, "A very efficient computer algorithm for direct frequency, aliasing and sensitivity analysis of SC networks," in *Proc. IEEE ISCAS Conf.*, Chicago, IL, Apr. 1981, pp. 864-876.
- [9] H. De Man, J. Rabaey, L. Claesen, and J. Vandewalle, "DIANA-SC: A complete CAD-system for switched capacitor filters," in *Proc. ESSCIRC Conf.*, Freiburg, Germany, Sept. 1981.
- [10] H. De Man, J. Rabaey, G. Arnout, and J. Vandewalle, "Practical implementation of a general computer-aided design technique for switched capacitor circuits," *IEEE J. Solid-State Circuits*, vol. SC-18, pp. 190-200, Apr. 1980.
- [11] L. W. Nagel, "Spice-2: A computer program to simulate semiconductor circuits," Univ. California Berkeley, CA, ERL. Memo N ERL M 520.
- [12] L. Chua and P. Lin, *Computer Aided Analysis of Electronic Circuits: Algorithms and Computational Techniques*. Englewood Cliffs, NJ: Prentice-Hall, 1975.
- [13] M. Schetzen, *The Volterra and Wiener Theory of Nonlinear Systems*. New York: Wiley, 1981.
- [14] L. Chua and C. Ng, "Frequency domain analysis of nonlinear systems: I, II," *Elec. Circuits Syst.*, vol. 3, pp. 165-185, 257-269, July 1979, Nov. 1979.
- [15] S. Narayanan, "Transistor distortion analysis using Volterra series representations," *Bell Syst. Tech. J.*, vol. 46, no. 5, pp. 991-1024, May-June 1967.
- [16] W. Vercruyssen, "Computer analyse van vervorming in filters met geschakelde capaciteiten," Masters thesis, Kath. Univ., Leuven, Belgium, June 1982.
- [17] D. Allstot, "MOS switched capacitor ladder filters," Univ. California Berkeley, CA, Memo No. UCB/ERL M79/30, May 1979.
- [18] D. Allstot, R. Brodersen, and P. Gray, "MOS switched capacitor ladder filters," *IEEE J. Solid-State Circuits*, vol. SC-13, pp. 806-814, Dec. 1978.
- [19] S. Chisholm and L. Nagel, "Efficient computer simulation of distortion in electronic circuits," *IEEE Trans. Circuit Theory*, vol. CT-20, pp. 742-745, Nov. 1973.



Joos Vandewalle (S'71-M'77-SM'82) was born in Kortrijk, Belgium, on August 31, 1948. He received the E.E. degree and the Ph.D. degree in applied sciences from the Katholieke Universiteit Leuven, Heverlee, Belgium, in 1971 and 1976, respectively.

From 1972 to 1976 he was Assistant at the ESAT Laboratory, Katholieke Universiteit Leuven. From 1976 to 1978, he was a Research Associate, and from July 1978 to July 1979 he was Visiting Assistant Professor at the University of California, Berkeley. Since July 1979 he has been back at the ESAT Laboratory of the Katholieke Universiteit Leuven, where he is Assistant Professor. His research interests are mainly in mathematical system theory and its applications in circuit theory, control, and data processing.



Ward Vercruyse was born in Roeselare, Belgium, on October 18, 1957. He received the E.E. degree from the Katholieke Universiteit Leuven, Heverlee, Belgium, in 1982.

In November 1982 he joined Silvar-Lisco, Heverlee, Belgium, where he is currently working in the field of simulation of switched capacitor circuits.



Jan Rabaey was born in Veurne, Belgium, on August 15, 1955. He received the E.E. degree from the Katholieke Universiteit Leuven, Heverlee, Belgium in 1978. He is currently finishing his work towards the Ph.D. degree on the theory, analysis and applications of switched capacitor filters in high quality audio filters.

In 1978, he obtained an I.W.O.N.L. fellowship, which allows him to work as a Research Assistant at the ESAT, Laboratory Katholieke Universiteit Leuven. In 1980 he obtained

a fellowship as NFWO Research Assistant.

Hugo J. De Man (M'81-SM'81), for a photograph and biography, see this issue, p. 266.

A Wide-Band Limiting Amplifier for Optical Fiber Repeaters

DAVID W. FAULKNER

Abstract—An integrated amplifier having a bandwidth of 470 MHz, and a gain and limiting range of 60 dB has been realized using a cascade of three cells on an uncommitted array. The circuit is capable of operating in optical fiber repeaters in the signal or retiming path at transmission rates up to 650 MBd. Direct expressions for calculating the gain and bandwidth have been derived which allow optimization of the component values, bias conditions, and transistor parameters for a chosen application.

I. INTRODUCTION

THE design objective was to produce a limiting amplifier compatible with a previously described single chip regenerator [1]. The requirements were 60 dB gain, a bandwidth in excess of 325 MHz, a limiting range of at least 40 dB, and a noise figure of better than 12 dB.

Manuscript received September 12, 1982; revised December 27, 1982. The author is with British Telecommunications Research Laboratories, Martlesham Heath, Ipswich, England.

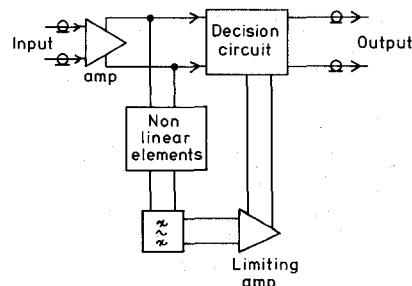


Fig. 1. Regenerator block diagram.

There are two functions in an optical fiber baseband repeater which can be met with wide-band limiting amplifiers. One is the gain in the transmission path prior to the decision gate and the other is gain in the retiming path following the timing extraction filter, as shown in Fig. 1. A gain of about 60 dB is required in both instances as the input signal is likely to